Remote Sensing of Temperature Profiles from a Combination of Observations from the Satellite-Based Microwave Sounding Unit and the Ground-Based Profiler

ED R. WESTWATER AND WANG ZHENHUI*

NOAA/ERL/Wave Propagation Laboratory, Boulder, CO 80303

NORMAN C. GRODY AND LARRY M. MCMILLIN

NOAA/NESDIS, Washington, D.C. 20233

(Manuscript received 11 June 1984, in final form 13 December 1984)

ABSTRACT

Temperature profiles are derived from ground- and satellite-based microwave radiometric observations. Data taken by the NOAA Profiler during December 1981 to December 1982, at Stapleton International Airport, Denver, Colorado, are combined with NOAA 6/7 Microwave Sounding Unit (MSU) observations over Denver. The results of 460 retrievals by the Profiler, the MSU, and the Profiler + MSU are compared with soundings by National Weather Service radiosondes (RAOBs). From the surface to 300 mb, maximum rms differences between the combined retrievals and RAOBs are less than about 2 K. For 17 cases in March 1981, radiometric data from the Profiler and MSU were combined with tropopause height measurements obtained from a VHF radar. The combined retrievals using the tropopause height information were improved in the vicinity of the tropopause by about 2 K rms relative to the pure passive ones.

1. Introduction

A ground-based remote sensing system to sound temperature, humidity and wind has been designed, constructed, and operated by the NOAA Wave Propagation Laboratory [Hogg *et al.*, 1983a]. This system, called the Profiler, was designed for unattended operation under nearly all-weather conditions and its operation for over two years in Denver, Colorado has met performance predictions in every regard. However, thermal soundings from the Profiler are poor (>2 K rms) above 500 mb, and need to be supplemented with another source of data. As suggested by Westwater and Grody (1980), the use of microwave data from satellites can improve retrievals above 500 mb. Conversely, below 500 mb, Profiler retrievals of both temperature and moisture can offer a substantial improvement over those of satellites. Therefore the value of Profiler systems will be enhanced if they form a national network of observing stations whose data are integrated with other sources of data, including soundings from both polar-orbiting and geostationary satellites [Little, 1982]. To evaluate the feasibility of such a comprehensive plan, the single-station accuracy of a combined satellite-Profiler system must be known. The principal objective of the present study is to determine experimentally the accuracies of temperature soundings obtained by a combined ground-based and orbiting satellite microwave radiometric system.

Earlier work, based on computer simulations, predicted that a combined ground-based and satellite microwave system could derive temperature profiles from the surface to about 300 mb with an rms accuracy of 1–2 K [Westwater and Grody, 1980]. In addition, if radar measurements of tropopause height were available, similar accuracies could be achieved up to 100 mb. In this paper, we derive temperature profiles by combining brightness temperature observations from the ground-based Profiler [Hogg *et al.*, 1983a] and from satellite observations by the Microwave Sounding Unit (MSU) aboard the NOAA 6/7 satellites [Grody, 1983]. Temperature retrievals using these data are compared with National Weather Service radiosonde observations (RAOBs) from Stapleton International Airport, Denver, Colorado. In all, we analyzed 460 joint Profiler-MSU-RAOB observations taken during the period December 1981 to December 1982. In an earlier work [Westwater *et al.*, 1984] Profiler retrievals were statistically combined with National Environmental Satellite, Data and Information Service (NESDIS) operational retrievals. Operational retrievals are derived from the complete TOVS (TIROS-N Operational Vertical Sounder) system that contains both infrared and microwave instruments [Phillips *et al.*, 1979]. The present study differs from the earlier one in three principal aspects:

* Permanent affiliation: Nanjing Institute of Meteorology, Nanjing, Peoples Republic of China.

a) Only the microwave data from the TOVS system are used. Although some information is lost by not including the infrared channels, both flexibility and simplicity are achieved in the design of retrieval algorithms when only microwave information is used. b) The *a priori* statistical inversion method, based on local climatological statistics, was used. The previous study used NESDIS operational retrievals, which are based on regression coefficients that are updated every two weeks. *A priori* methods can be used with the microwave data because in this frequency region brightness temperatures can be accurately calculated from RAOBs [see Section 3]. With this method, no updating is necessary. c) We compared Profiler accuracies not only with MSU retrievals but also with retrievals based on MSU and surface meteorological data. Thus the information added to a combined retrieval by the addition of the Profiler's radiometric channels can be evaluated.

In addition to the passive microwave retrievals, we also analyzed data taken during March 1981 in which VHF radar observations of tropopause height were available. As we show in Sec. 6, properly measured tropopause heights can be used to improve temperature retrievals significantly in the vicinity of the tropopause.

2. Description of instruments

The Profiler is a ground-based remote sensing system designed to measure profiles of wind and temperature as well as integrated water vapor and cloud liquid. Instrumental details of this system and its initial remote sounding results are extensively described by Hogg *et al.* (1983a). Below, we describe briefly the portion of the instrumentation that we use in this paper.

The Profiler is less than 100 m from the National Weather Service (NWS) radiosonde launch site. The Profiler's six-channel radiometer has one channel operating at 20.6 GHz, one at 31.65 GHz and four channels between 50 and 60 GHz. All six channels have equal beamwidths of 2.3° and the instrument only views in the zenith direction. The two lower channels are used to derive precipitable water and cloud liquid and also to provide corrections for these variables to the 50–60 GHz temperature channels. Data from the six channels, supplemented with surface measurements of pressure, temperature, and relative humidity, are converted to profiles of temperature and humidity by linear statistical inversion. The details of our profile retrieval algorithms are discussed in Sec. 4.

Although 2-min samples of profile retrievals are derived and archived, we use 20-min averages for combination with the satellite data and comparison with radiosonde data. For the RAOB comparison, the time average starts at the time of radiosonde release.

The data processing for the Profiler eliminates strong cloud and rain effects by rejecting data for which the 31 GHz brightness temperature exceeds 100 K, which is roughly equivalent to a cloud liquid amount of 2 mm. This threshold was exceeded for 3 of the 460 cases we analyze in Sec. 5 and 6. In these three cases, we replaced the deleted data with those from another 20-min period within ±1 h of radiosonde launch time. For all other data, no additional processing was necessary.

The Microwave Sounding Unit is a component of an operational sounding system and was designed 1) to produce global temperature soundings under nearly all weather conditions and 2) to complement an infrared sounder that contains more channels but is limited to clearer atmospheres (Smith *et al.*, 1979). First launched on 13 October 1978 aboard the polar orbiting TIROS-N satellite (later aboard NOAA satellites), the MSU contains four channels in the oxygen band, at 50.30, 53.74, 54.96, and 57.95 GHz, to provide temperature profile information from the lower troposphere to the lower stratosphere. Further details of this instrument, including its scan pattern, are given by Grody (1983).

The brightness temperature $T_b(\nu)$, at frequency ν, observed by the Profiler or the MSU is related to the vertical temperature profile $T(h)$, where h = height, by an equation of the form

$$T_b(\nu) = \int_0^\infty T(h)W(\nu, h)dh + T_{\mathrm{BACK}}(\nu)e^{-\tau(\nu)}. \quad (1)$$

Here $W(\nu, h)$ is the so-called temperature weighting function, $T_{\mathrm{BACK}}(\nu)$ is a background brightness temperature, and $\tau(\nu)$ is the opacity from Earth to space. For upward-looking observations, $T_{\mathrm{BACK}}(\nu)$ describes the "big bang" cosmic background of 2.9 K, as well as emission from discrete sources. For downward-looking observations, $T_{\mathrm{BACK}}(\nu)$ describes reflected and emitted radiation from the Earth's surface. Equation (1) is valid only for a non-scattering atmosphere, which precludes its use when large precipitation particles are present. Profiler and MSU temperature weighting functions, calculated from the U.S. Standard Atmosphere, are shown in Fig. 1. Note how the Profiler capabilities, which are exponentially reduced above 500 mb, are complemented by the MSU; conversely, note how the relatively high vertical resolution at lower altitudes of the Profiler complements the MSU below 500 mb.

In addition to differences in vertical coverage between the Profiler and MSU, as quantified by the weighting functions of Fig. 1, differences in horizontal resolution are also important. The beamwidths of the MSU channels are 7.5°, which results in a nadir footprint of 110 km from the nominal 833 km orbiting altitude. At the extremes of the beam scan, the footprint has enlarged to an elliptical shape of axis dimension ~180 × 325 km. The Profiler with

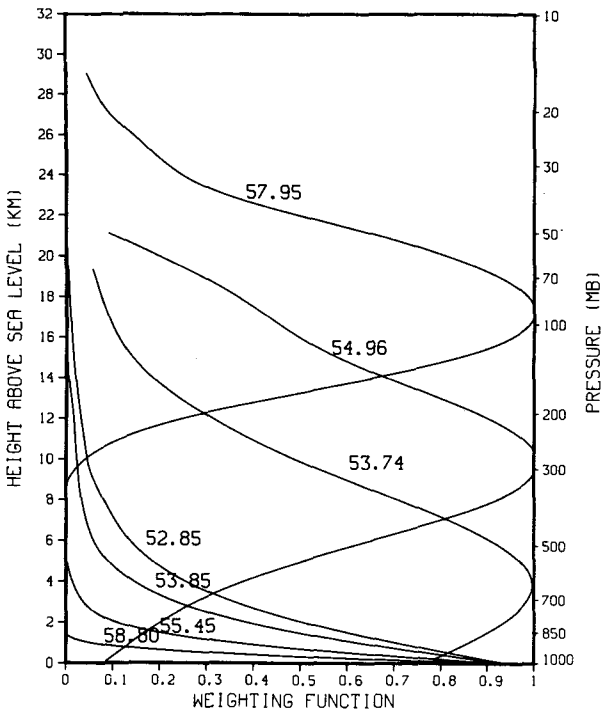

FIG. 1. Temperature weighting functions, in relative units, for the Profiler and the MSU. The upper three curves are for the MSU; the lower four curves are for the Profiler.

its 2.3° beam, will observe an area of about 400 m at 10 km altitude. Thus the Profiler and the satellite represent completely different spatial scales. When combining Profiler and satellite data to derive profiles, problems could arise when the atmosphere exhibits strong departures from horizontal stratification. Such departures occur in the boundary layer, during strong convective storms and during the passage of frontal systems. Although a complete analysis of each of these effects is beyond the scope of this paper, the following reasonable argument can be made: in the lower troposphere, the Profiler dominates the combined retrieval; in the upper troposphere and stratosphere, the MSU dominates the combined retrieval. Therefore, departures from stratification in the lower troposphere, at least, will have only a minor effect on the combined retrievals.

3. MSU data interpretation

The MSU brightness temperature measurements for our study were supplied by NOAA/NESDIS. The data processing program contains a standard limb correction procedure for removing the effect of angular scanning on the measurements. This procedure, developed by Smith *et al.* (1979), uses regression equations to compute the nadir brightness temperature of a given channel from a linear combination of all channel measurements at a particular scan angle. Synthesized clear and cloudy brightness temperatures computed from a climatological set of atmospheres are used to derive the regression equations. This method of modifying the measurements to nadir values is applied operationally in processing MSU data and was used in this study. However, the climatological set of atmospheres used in deriving the regression equations was composed of radiosondes, whose surface altitudes were generally near sea level. As we show below, in using MSU data taken over Denver, Colorado (altitude = 1.611 km), further corrections were necessary.

A necessary condition for most profile retrieval techniques, including ours (see Sec. 4), is the ability to calculate brightness temperature as a function of environmental parameters. Within the constraints of our data set of Denver RAOBs and satellite measurements, we compare measurements and calculations to determine the "effective" accuracy of the measurements. The upwelling microwave brightness temperature depends on profiles of temperature and water vapor which are measured by RAOBs. Using these profiles we calculate oxygen absorption, following Rosenkranz (1975), and water vapor absorption, following Hogg *et al.* (1983b). The thermal emission also depends on cloud liquid, surface skin temperature, and emissivity, parameters that are not available from RAOBs. However, we can compare measurements and calculations on profiles for which cloud emission is small. According to the NESDIS sounding classification (Phillips *et al.*, 1979), three types of operational retrievals are available for the complete TOVS system—clear, partly cloudy, and cloudy. For the first two of these categories, surface skin temperature is available, and we make the assumption that we could neglect clouds in this ensemble. The 460 profiles that comprise our data set (see Sec. 5) were classified as 216 clear, 173 partly cloudy, and 71 cloudy. We initially made comparisons of measurements and calculations on the complete clear and partly cloudy data sets. However, it was quickly discovered that not all of these data were suitable for direct problem comparisons. There were a substantial number of "short" RAOB soundings; i.e., soundings that did not extend to 30 mb. Even after a standard atmosphere was used to extrapolate the short soundings to 0.1 mb, sometimes 5–10 K differences existed at the upper two MSU channels between measurements and calculations. Therefore, we eliminated from the data set used in the direct problem calculations all soundings that did not extend to 30 mb. The number of clear and partly cloudy soundings in this data set is 221. Within this restricted data set, we have most of the elements from which upwelling brightness can be calculated. Our procedure, that we outline below, is to calculate atmosphere radiance from RAOBs, to obtain skin temperature from the TOVS operational products, and to derive emissivity from 50.3 GHz MSU measurements. Only satellite data within ±3 h of RAOB release time were used.

The brightness temperature T_b^m observed by a satellite in the absence of atmospheric scattering is given by

$$T_b^m = T_s\epsilon_s e^{-\tau} + (1 - \epsilon_s)\overline{T_b^{\downarrow}}e^{-\tau} + T_b^{\uparrow} \qquad (2)$$

where

T_s = skin temperature (K)
$\overline{T_b^{\downarrow}}$ = weighted angular average of downwelling brightness temperature (K)
$T_b^{\uparrow}$ = upwelling brightness temperature (K)
ϵ_s = surface emissivity
τ = opacity (nepers).

In Eq. (2) the first term represents surface emission while the third is the upwelling atmospheric emission. The second term is a suitably averaged brightness temperature representing downwelling radiation scattered from the Earth's surface. It is usual in atmospheric microwave radiometry to assume specular reflection at the Earth's surface (Grody, 1983), i.e.,

$$\overline{T_b^{\downarrow}}(\theta) = T_b^{\uparrow}(\theta),$$

where θ is the nadir viewing angle of the satellite. The MSU channel which is most sensitive to surface variation, and hence to the assumption of specular reflection, is 50.3 GHz. At this frequency, differences in T_b^m at nadir between specular reflection and scattering that obeys a cosine law were calculated to be about 3 K. In the following, we will assume specular reflection, and over the 50–60 GHz frequency interval, assume that ϵ_s is independent of frequency. We solve Eq. (2) for ϵ_s to obtain

$$\epsilon_s = \frac{T_b^m - T_b^{\uparrow} - T_b^{\downarrow}e^{-\tau}}{(T_s - T_b^{\downarrow})e^{-\tau}}. \qquad (3)$$

With our restriction to noncloudy or light-cloudy conditions, we can compute $T_b^{\uparrow}$, $T_b^{\downarrow}$, and τ from RAOBs, get T_s from the operational retrievals, and thus derive ϵ_s from 50.30 GHz T_b measurements. This value of ϵ_s (and T_s) can then be inserted into Eq. (2) to compare measurements and calculations at the temperature sounding channels. The difference in calculated emissivities assuming a specular law or a cosine law was about 2%. This small difference would have a negligible impact on the temperature sounding channels. We also made comparisons with T_b's that were calculated assuming ϵ_s = 1.0 and 0.9. Comparisons of measured (T_b^m) and calculated (T_b^c) are given in Table 1. As can be expected from a cursory look at the temperature weighting functions in Fig. 1, only the sounding channel at 53.74 GHz is affected by surface conditions. We observe that on the average, measurements are colder than calculations at all three channels. The comparisons agree with Grody (1983) for channels 2 (C2) and 3 (C3), but differ in sign for channel 4 (C4).

Grody's (1983) results also indicated that, for at least one channel, the regression line between T_b^m and T_b^c, had a nonunity slope. To compare with his

TABLE 1. Comparison of calculated and satellite-measured brightness temperature $T_b^c - T_b^m$ (K) for various choices of surface emissivity ϵ_s. C2 = 53.74, C3 = 54.96 and C4 = 57.95 GHz. Sample size = 221.

		ϵ_s		
Channel		by Eq. 3	1.0	0.9
C2	Average	0.96	1.83	0.58
	Standard deviation	1.02	1.28	1.18
C3	Average	1.74	1.75	1.74
	Standard deviation	0.78	0.78	0.78
C4	Average	0.49	0.49	0.49
	Standard deviation	1.04	1.04	1.04

results we also performed regression analysis on our data. However, interpretation of these regression analyses requires some discussion. A measurement of brightness temperature departs from the "true value" by both a fluctuating part, due to receiver noise, etc., and a bias portion, due to a variety of causes, such as calibration uncertainties, finite beam width, etc. On the other hand, calculations of emission temperature are based on radiosonde observations, which are themselves in error, and on absorption equations that are only an approximation to nature. In addition, there are spatial and temporal differences between RAOB and radiometer that lead to discrepancies that are difficult to associate with either quantity individually. Thus, in the comparison of T_b^m and T_b^c, one has the classic case of both variables containing errors and hence, strictly speaking, standard regression analysis does not apply. Consequently we computed for our data set three regression relations that assume, respectively, 1) T_b^c is exact and T_b^m contains error:

$$\hat{T}_b^m = A + BT_b^c \qquad (4)$$

where

$$A = \overline{T_b^m} - B\overline{T_b^c}$$

and

$$B = \frac{\mathrm{cov}(T_b^m, T_b^c)}{\mathrm{var}(T_b^c)};$$

2) T_b^m is exact and T_b^c contains error:

$$\hat{T}_b^c = a + bT_b^m \qquad (5)$$

where

$$a = \overline{T_b^c} - b\overline{T_b^m}$$

and

$$b = \frac{\mathrm{cov}(T_b^m, T_b^c)}{\mathrm{var}(T_b^m)};$$

and 3) both variables contain error:

$$T_b^c = \alpha + \beta T_b^m \qquad (6)$$

or

$$T_b^m = -(\alpha/\beta) + \frac{1}{\beta}(T_b^c).$$

In Eq. (6), α and β were determined from equations given in Kendall and Stuart (1967):

$$\left.\begin{aligned}\alpha &= \overline{T_b^c} - \beta\overline{T_b^m},\\ \beta &= \frac{D + (D^2 - 4\lambda C^2)^{1/2}}{2C}\end{aligned}\right\}$$

where

$$\left.\begin{aligned}D &= \lambda(\mathrm{var}T_b^m - \mathrm{var}T_b^c)\\ C &= \mathrm{cov}(T_b^m, T_b^c)\end{aligned}\right\}.$$

In Eqs. (4)–(6) var and cov refer to the statistical functions variance and covariance, and the overbars to ensemble averages. The parameter λ is the ratio of the (unknown) error variances in T_b^c and T_b^m and must be assumed. We computed α and β under two assumptions: $\lambda = 1$ and $\lambda = \mathrm{var}T_b^m/\mathrm{var}T_b^c$. For these choices the slopes differed only in the third decimal place. In the following, we will show only the regression fits assuming error in both variables for $\lambda = 1$. We plot the regression lines of Eqs. (4)–(6) and show the associated scatter plots in Fig. 2. The regression lines and their statistical uncertainties are also shown in Table 2. We observe that both C3 and C4 exhibit slopes that depart from unity; note, however, the result of C4 when T_b^m is a predictor. In addition to these regression equations for the composite data of both satellites, we derived similar equations for the separate NOAA 6 and NOAA 7 satellites. These data yielded essentially the same constants as Table 2. Our absorption algorithms were compared with those of Grody (1983), and the results of T_b calculations were within 0.1 K. Thus although the reason for the nonunity slopes is not clear, the results of the standard errors of prediction clearly shows that with proper calibration, rms brightness temperature accuracies of 1 K are achievable.

In Sec. 5, we derive temperature profiles from satellite T_b measurements. Our retrieval algorithms (discussed in Sec. 4) require knowledge of radiometric noise levels, or more specifically, the noise covariance matrix. To estimate this covariance matrix in a manner that allowed us to perform completely independent retrievals, we divided our data by random number generation into two sets. For each set, we computed

1) the linear-least-squares fit for each channel; e.g.,

$$\hat{T}_b^c = AT_b^m + B,$$

(using T_b^c as our "effective" measurement, since our profile retrieval coefficients are based on calculated data);

2) the noise covariance matrix S_ξ

$$(S_\xi)_{ij} = \frac{1}{N-2}\sum_{k=1}^{N}(T_b^c - \hat{T}_b^c)_i(T_b^c - \hat{T}_b^c)_j,$$

$$i, j = 1, 2, 3$$

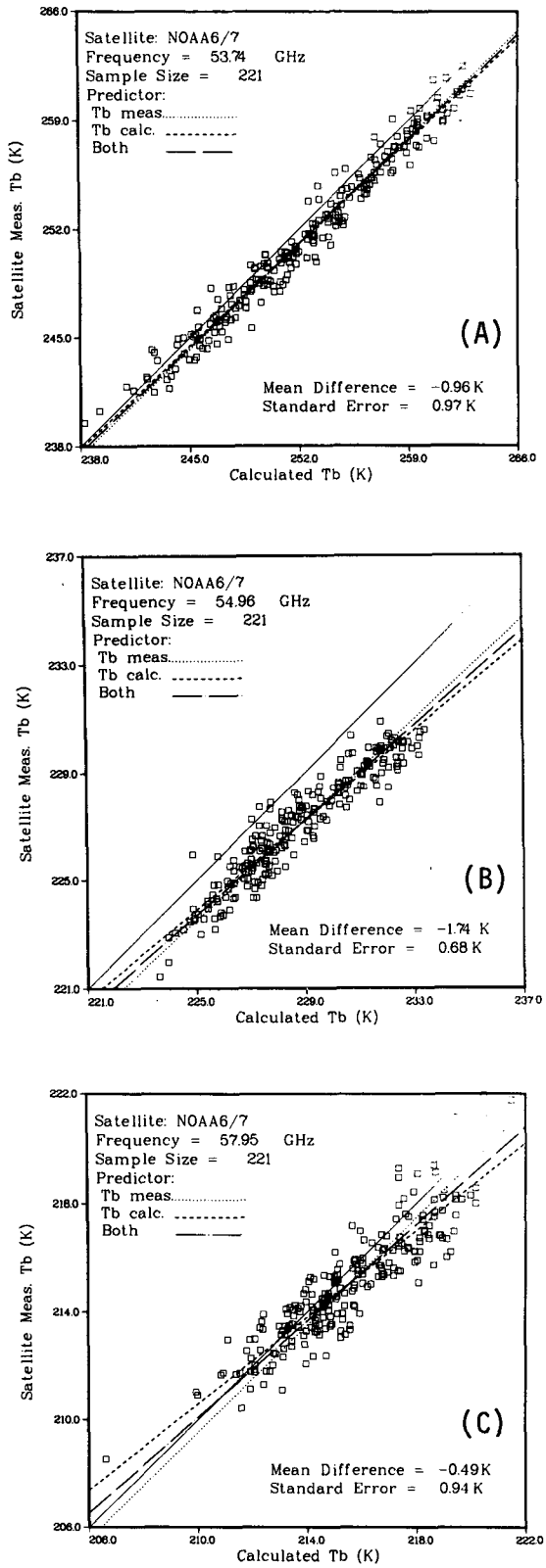

FIG. 2. Comparison of measured and calculated brightness temperatures for (a) channel 2 (b) channel 3 and (c) channel 4 of the MSU. The differences between the three regression lines in each figure are discussed in the text.

TABLE 2. Regression analysis of measured (T_b^m) and calculated (T_b^c) brightness temperatures where T_b (predicted) $= A + B \cdot \hat{T}_b$ (predictor). Sample size = 221.

Channel number	Predictor		A (K)	B	Standard error (K)
C2		T_b^c	13.4 ± 3.0	0.943 ± 0.012	0.97
		T_b^m	−5.0 ± 3.3	1.024 ± 0.013	1.02
	both*	T_b^c	9.4	0.959	
		T_b^m	−9.8	1.043	
C3		T_b^c	36.8 ± 4.5	0.831 ± 0.020	0.68
		T_b^m	−14.9 ± 5.7	1.073 ± 0.025	0.76
	both*	T_b^c	27.2	0.874	
		T_b^m	−31.1	1.145	
C4		T_b^c	41.8 ± 5.7	0.804 ± 0.026	0.94
		T_b^m	−0.9 ± 7.1	1.007 ± 0.033	1.05
	both*	T_b^c	24.8	0.883	
		T_b^m	−28.1	1.133	

* Refers to regression assuming both variables are predictors.

and 3) retrieval coefficients (see Sec. 4). Finally, each set of retrieval coefficients was applied to its complementary set of data. The noise covariance matrix for the entire (non-divided) data set is given in Table 3.

4. Retrieval method

Our method of deriving temperature and humidity profiles from observed brightness temperature was linear *a priori* statistical inversion [Strand and Westwater, 1968]. When used at a location for which a history of RAOBs is available, this method has some attractive features. The first is that local climatological conditions can be adequately modeled. Another is the ease with which profiles can be constrained and restricted by surface measurements. Finally, if a large data base of profiles is available, this ensemble can be stratified into meteorologically identifiable subsets, each of which contains an adequate sample size of representative profiles. An example of this stratification is one based on tropopause height (see Sec. 6).

With the *a priori* method, a profile vector $\mathbf{p}$ is estimated from a measured data vector $\mathbf{d}$ by

$$\mathbf{p} = \langle \mathbf{p} \rangle + \langle \mathbf{p}'\mathbf{d}'^T \rangle \langle \mathbf{d}'\mathbf{d}'^T \rangle^{-1} (\mathbf{d} - \langle \mathbf{d} \rangle) \qquad (7)$$

where $\langle\ \rangle$ represents ensemble averaging over a joint distribution of profiles and experimental noise, $\mathbf{v}^T$ is the matrix transpose of the column vector $\mathbf{v}$, and the primes refer to departures from ensemble average; e.g., $\mathbf{v}' = \mathbf{v} - \langle \mathbf{v} \rangle$. In Eq. (7), $\mathbf{d}$ is the sum of a true part and a measurement error ξ.

The ensembles used to determine our retrieval coefficients were selected from NWS RAOBs taken at Denver, Colorado during 1972–1977. For the ith month ($i = 1, 2, \ldots, 12$) coefficients were computed on data representing the months ($i - 1$), i, and ($i + 1$). Clouds were simulated following Decker *et al.* (1978), and Profiler noise levels were chosen following Hogg *et al.* (1983a). The MSU noise levels (S_ξ) were assumed independent of the Profiler and were determined from the covariance matrices computed as described in Sec. 3. To determine the three (correlated) components of noise for a particular realization of simulated MSU T_b's, three independent random normal deviates ξ (with zero mean and unit standard deviation) were transformed into variables having the appropriate covariance. This transformation was accomplished by Cholesky decomposition (Dongarra *et al.*, 1979). If ξ_{MSU} is the simulated MSU noise vector and $\mathbf{I}$ the identity matrix, then

$$\xi^{\mathrm{MSU}} = A\xi \qquad (8)$$

where

$$\left.\begin{aligned} AA^T &= S_\xi \\ \langle ;\xi\xi^T \rangle &= \mathbf{I} \end{aligned}\right\}.$$

5. Results of temperature retrieval by combining MSU and Profiler data

In order to compare and combine Profiler and MSU retrievals, our data base consisted of NWS RAOBs, 20-min averages of Profiler data, starting at RAOB release time, and NOAA 6/7 measurements over the Denver, Colorado area. The satellite data were restricted to be within ±3 h from 00 to 12 GMT and to fall within an area −0.5 to +1.0°N and 0.0 to +2.0°E of the joint NWS-Profiler site at 39°46′N latitude and 104°53′W longitude. The area included the plains east and north of Denver and excluded all of the Rocky Mountains. For the time period December 1981–December 1982, we were able to obtain 460 RAOB-Profiler-MSU data cases. This number of cases is considerably less than the possible ~1460 from the twice-a-day overflights of the two satellites. The reduction is primarily due to the geographical restriction of lying completely east of the Rockies, although some data were not available due to equipment outages. However, no data were excluded because of adverse weather effects on either the Profiler or the MSU data.

Using Eq. (7) we derived temperature profiles from various choices of data vectors whose components are shown in Table 4. Thus, we retrieved profiles

TABLE 3. Noise covariance matrix (K^2) determined by a comparison of calculated and measured brightness temperatures. Sample size = 221. C2 = 53.74, C3 = 54.96 and C4 = 57.95 GHz.

Channel	C2	C3	C4
C2	1.03	0.18	0.04
C3	0.18	0.59	0.33
C4	0.04	0.33	1.10

TABLE 4. Components of data vectors used in temperature and water vapor profile retrieval. T_s = surface temperature (°C); P_s = surface pressure (mb); RH_s = surface relative humidity; $T_{b,P}$ = Profiler brightness temperature (K); T_{bMSU} = MSU brightness temperature (K); τ_P = optical depth (nepers). Values in parentheses indicate frequencies in GHz.

Component number	Profiler	MSU	MSU + Surface Meteor.	Profiler + MSU
1	T_s	$T_{b,MSU}$ (53.74)	$T_{b,MSU}$ (53.74)	T_s
2	P_s	$T_{b,MSU}$ (54.96)	$T_{b,MSU}$ (54.96)	P_s
3	RH_s	$T_{b,MSU}$ (57.95)	$T_{b,MSU}$ (57.95)	RH_s
4	$T_{b,P}$ (53.85)		T_s	$T_{b,P}$ (53.85)
5	$T_{b,P}$ (55.45)		P_s	$T_{b,P}$ (55.45)
6	$T_{b,P}$ (58.80)		RH_s	$T_{b,P}$ (58.80)
7	τ_P (20.6)			τ_P (20.6)
8	τ_P (31.65)			τ_P (31.65)
9	$T_{b,P}$ (52.80)			$T_{b,P}$ (52.80)
10				$T_{b,MSU}$ (53.74)
11				$T_{b,MSU}$ (54.96)
12				$T_{b,MSU}$ (57.95)

using data from the 1) Profiler 2) MSU 3) MSU + surface meteorological measurements and 4) Profiler + MSU. Selected retrieval results for each of these systems are compared with RAOBs in Fig. 3. We note, as expected, that results for the combined Profiler + MSU are generally superior to either of its separate components. The combined Profiler + MSU results tend to be close to those of the Profiler in the lower atmosphere but do not necessarily follow the MSU at, say, pressures less than 300 mb. Two of the worst retrievals in the entire data set are shown in Figs. 3c, d. In Fig. 3c, the sharp "bulge" in temperature at the 250–100 mb region is not resolved by any of the systems. Figure 3d shows the poor recovery of a sharp elevated inversion (ΔT = 15°C) whose base is at 700 mb. For some applications, these deficiencies are serious.

The total rms difference statistics, relative to RAOBs, in temperature for each of the four retrieval types are shown in Fig. 4a. As a baseline value, we also show the rms variation using surface meteorological measurements as predictors. We note that the MSU + Profiler results are everywhere more accurate than any of the separate subsystems. This is not trivial, since if we had incorrectly modeled relative covariance, for example, combined retrievals might be poorer than the separate ones. A curious feature presents itself in the combination of MSU and surface data. As expected, surface predictors (namely surface temperature) improve retrieval accuracy in the first $\approx$100 mb above the surface. However, in the 400–200 mb region, surface data improve accuracy by as much as 0.5 K. As suggested by Westwater and Grody (1980), this improvement results from a correlation of surface pressure with the temperature aloft. We also observe that the retrieval results of all the systems improve substantially over predictions based on surface climatology, except for the MSU in the lowest 50 mb. For completeness, we show the average difference between RAOB and retrievals in Fig. 4b.

Some of the rms differences between MSU retrievals and RAOBs are due to temporal differences in the respective measurements within the ±3 hr window. Especially significant are boundary layer changes due to surface heating and cooling. To estimate the magnitude of these effects, Westwater *et al.* (1984) compared Profiler retrievals with RAOBs at a) RAOB release time and b) the time of satellite overflight. These results showed noticeable differences only in the lowest ~150 mb. However in the lowest 50 mb, 2–4 K rms differences were observed.

In addition to temperature retrievals, we derived geopotential heights and thicknesses for the various systems. These quantities also depend on water vapor, a quantity derived by the Profiler but not by the MSU. To derive pressure heights from the MSU data, we used monthly mean water vapor profiles with the MSU-derived temperature profiles and vapor profiles estimated from surface data with the (MSU + surface)-derived temperature. Retrievals of all systems used RAOB surface pressure as a reference. These results of the geopotential heights and thickness determinations are given in Tables 5 and 6. In Table 5, we also present the estimated functional precision of radiosondes, as given by Hoehne (1980). His original values were taken at sea level and required an adjustment (about 6 m downward) to Denver's surface pressure. That this adjustment is approximate is shown by both the Profiler and Profiler + MSU results being better than the RAOB precision at 700 mb. From these tables, we observe that the Profiler + MSU results are a significant improvement over the Profiler's, primarily in the 300–100 mb range. Scatter plots of the entire data set for the MSU + surface, Profiler, and Profiler + MSU are shown in Fig. 5 for rms pressure-height comparisons and in Fig. 6 for rms thickness comparisons. It is evident from these figures that no significant departures from linearity are evident over a considerable range of variation of the data.

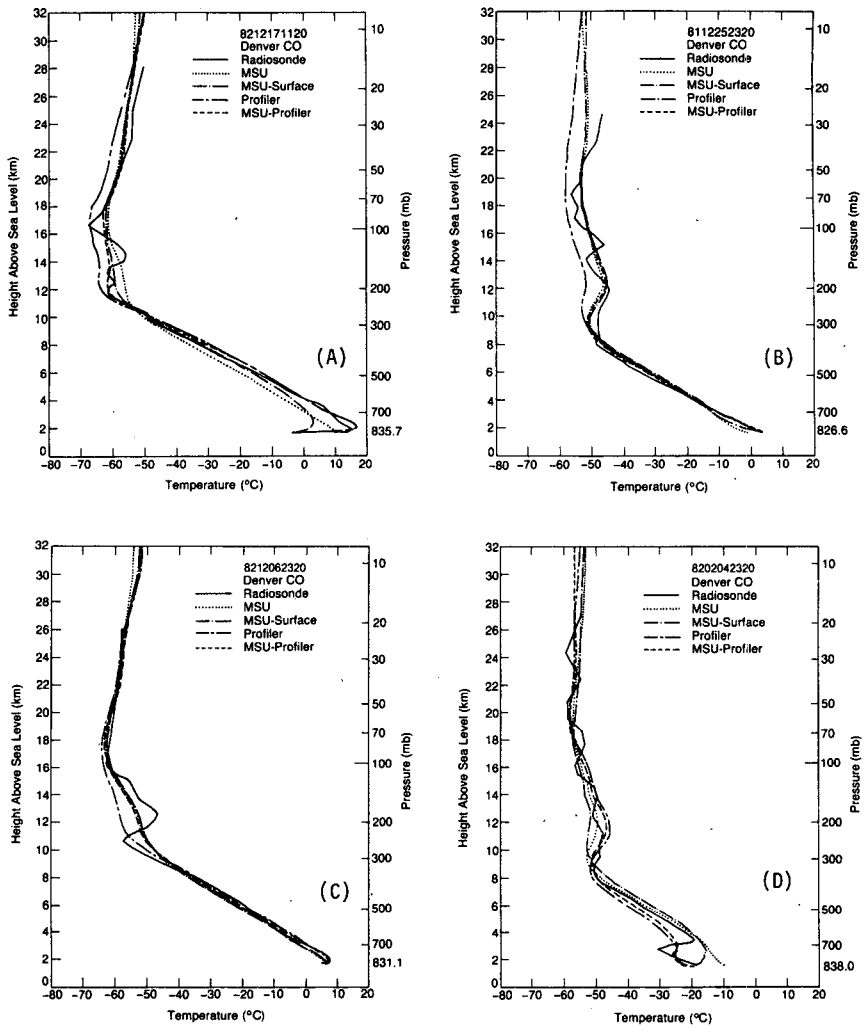

FIG. 3. Selected comparisons of RAOB temperature profiles with those derived from various combinations of Profiler and MSU observations.

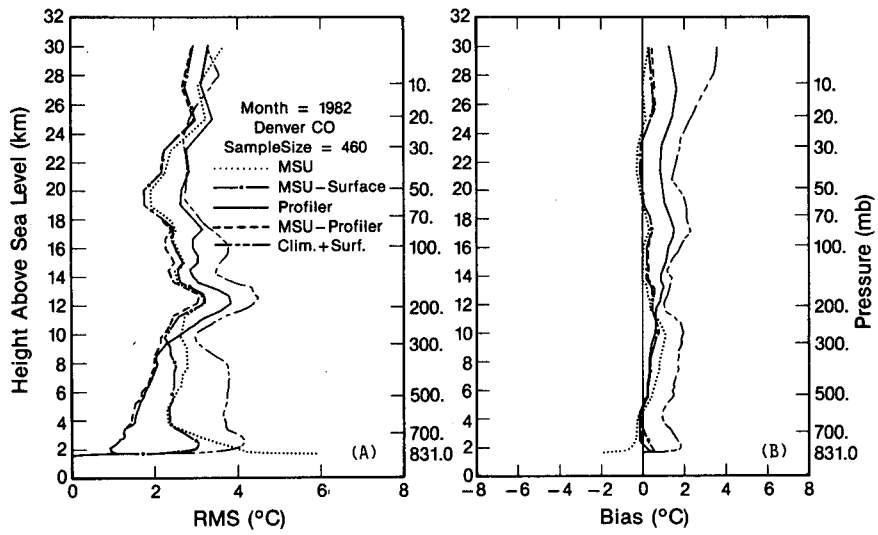

FIG. 4. Statistics of differences between RAOBs and retrievals: (a) total rms differences (b) biases. Bias refers to RAOB-retrieval.

TABLE 5. The rms differences relative to RAOBs in determination of geopotential height (m) for various combinations of remote sensing systems.

Pressure level (mb)	Climatology (monthly means)	Surface meteorology	MSU	MSU + surface	Profiler	MSU + profiler	Functional precision of radiosondes (Hoehne, 1980)
700 (N = 458)	32.2	18.7	17.2	13.5	3.8	3.8	5.1
500 (N = 458)	71.3	49.6	32.2	31.2	13.1	12.4	12.7
300 (N = 456)	117.9	89.5	57.3	56.9	33.0	31.1	20.3
100 (N = 446)	93.1	74.3	60.6	51.7	67.6	46.0	27.9

6. Combined radar–radiometric temperature retrievals

Studies have shown that VHF radars can measure the height of the tropopause (Gage and Green, 1979). As predicted theoretically by Westwater and Grody (1980) and verified experimentally (Westwater *et al.*, 1983), the tropopause height information can be used to improve temperature retrieval accuracy of radiometric sensors. In this section, we will show examples of the combined passive–active techniques for a small data set taken during March 1981.

The VHF radar is located at the Platteville (Colorado) Radar Facility, about 50 km north of Denver, and is operated jointly by the NOAA/Aeronomy Laboratory and the NOAA/Wave Propagation Laboratory. The primary purpose of the radar is to measure all three components of winds. However, during the month of March 1981, the radar was operated only in the vertical sounding mode to achieve a higher than usual sampling rate. Tropopause heights are derived from the vertical sounding data using the algorithms given by Westwater *et al.* (1983). In particular the so-called RC (reflectivity correlation) method that we use is described there. Pertinent system parameters of this radar are listed in Table 7.

We were able to compare temperature retrievals for three passive systems (Profiler, MSU, and Profiler + MSU) and three passive + active systems (each passive system plus VHF radar). Our retrieval algorithms used to incorporate active and passive measurements is a straightforward generalization of the method given in Sec. 4 and is described by Westwater *et al.* (1983). Again, an experimentally determined covariance matrix was used to simulate satellite noise levels.

Sample profiles derived from various combinations of sounding systems are shown in Fig. 7a–f. Note that in Fig. 7a, b the ground-based radiometer retrieval closely matches the radiosonde up to about 10 km, but then departs by several degrees from the sonde. Also note the improvement added when the tropopause information from the VHF radar is introduced. In Fig. 7c, d, the MSU retrieval is much closer to the radiosonde in the tropopause region, but is seriously in error below about 600 mb. Again, as for the ground-based radiometer, the tropopause height measurement adds structure in the 100–200 mb region. Finally, Fig. 7e, f shows a combined retrieval (ground- and satellite-based) that is superior in accuracy to either of the separate retrievals.

The rms differences for the three combinations are shown in Fig. 8a–c:

Figure 8a. Ground-based radiometer and VHF radar. Note the large improvement in retrieval accuracy, ~2 K rms, near tropopause pressures (300 to 100 mb) when tropopause height measurements are

TABLE 6. The rms differences relative to RAOBs in determination of geopotential thickness (m) for various combinations of remote sensing systems.

Pressure level (mb)	Climatology (monthly mean)	Surface meteorology	MSU	MSU + surface	Profiler	MSU + profiler
700–500 (N = 458)	42.0	33.3	21.0	21.4	12.4	11.5
500–300 (N = 456)	53.7	45.3	37.8	33.6	26.4	25.6
300–100 (N = 446)	85.7	82.2	47.5	47.9	65.8	42.9

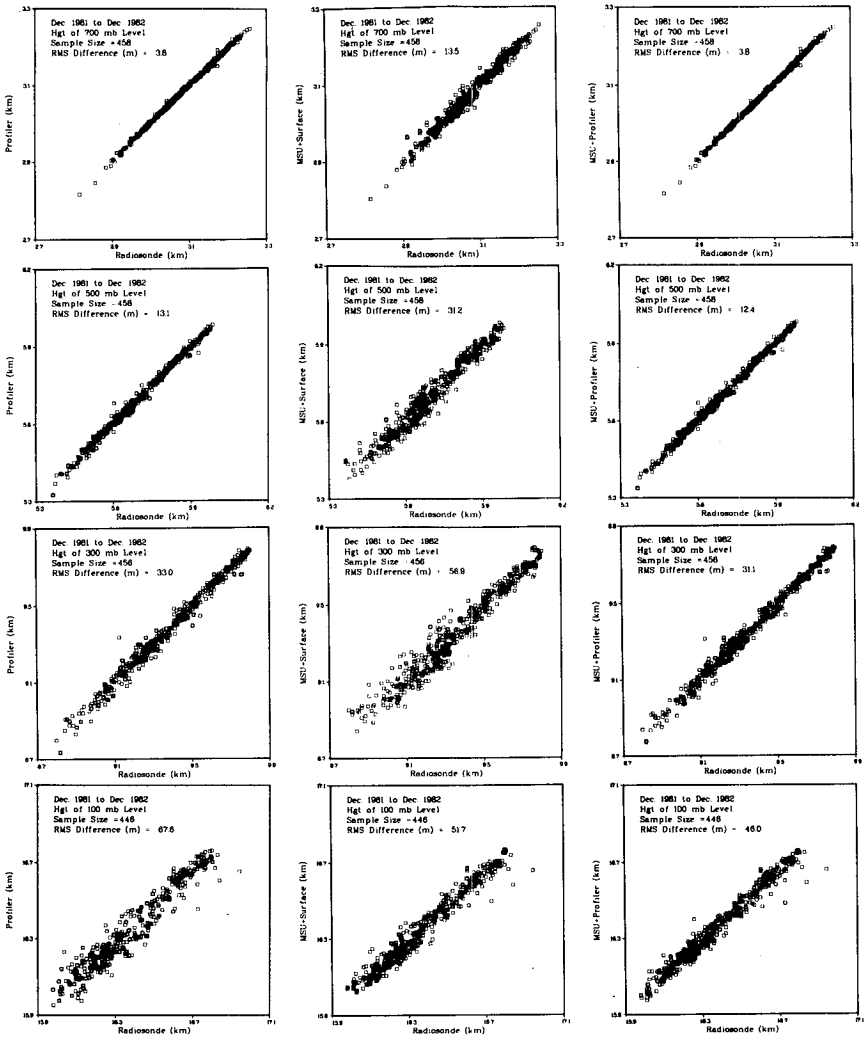

FIG. 5. Scatter plots of geopotential heights at 700, 500, 300, and 100 mb as measured by NWS RAOBs at Denver, CO and heights determined from retrievals by Profiler, MSU + surface, and Profiler + MSU.

added. However, retrieval accuracy above 300 mb is poor.

Figure 8b. Satellite-based radiometer (MSU) + VHF radar. Again, note ~2 K rms improvement of MSU results when the tropopause height measurements are inserted. Here, retrieval accuracy below about 700 mb ranges from almost 3 to 6 K rms.

Figure 8c. Ground-based radiometer + VHF radar + MSU. The solid curve, representing the combined radiometric systems, shows improvement over either of the pure radiometric results of Fig. 8a or b, except in the vicinity of the tropopause. A further increase in accuracy is achieved by adding the radar measurements of tropopause height, as shown by the dashed curve in this figure. Except for a narrow pressure region near 200 mb, the rms differences from the surface to 30 mb are less than 2 K.

7. Conclusions and discussions

Computer simulations by Westwater and Grody (1980) showed that a combination of ground-based and satellite microwave radiometers could lead to an effective temperature–sensing system by overcoming some of the separate weaknesses of each system. These predictions showed the accuracy of the ground-based system degrades rapidly above 500 mb, a region where the MSU retrieval accuracy is good; conversely, the MSU accuracy is poor below 500 mb, a region of good coverage by the Profiler. Our experimentally achieved rms temperature retrieval errors, based on 460 cases, are close to the earlier theoretical predictions.

Passive temperature retrievals from the combined ground-based radiometers and MSU demonstrated

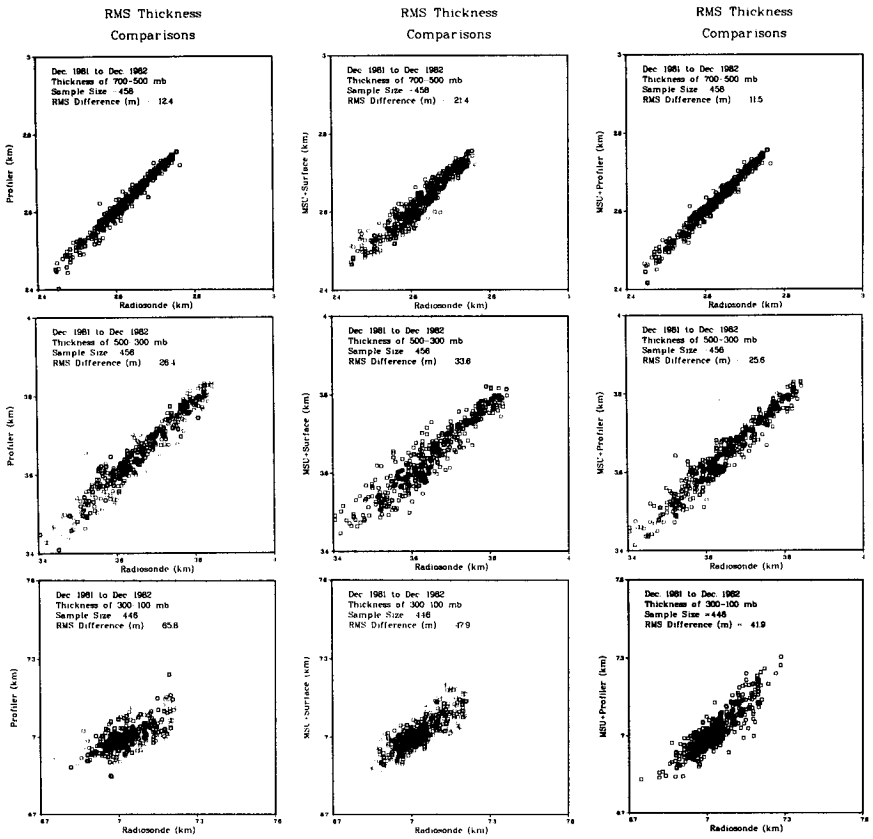

FIG. 6. Scatter plots of thickness of the pressure layers 700–500, 500–300 and 300–100 mb. Data are from the same three systems as in Fig. 5.

accuracy that is approaching operational requirements for synoptic scale numerical forecasting. Retrievals of geopotential heights, in the lowest 500 mb, are competitive with those from radiosondes. However, as with most passive retrievals, the vertical resolution of recovered profiles is poor. We have shown here that tropopause height information obtained from an active sensor (VHF radar) improved the resolution of profiles derived from each of three separate sensors. An analysis of this technique, using a much larger data set than that of March 1981, is now under way. In addition to improving profiles by using tropopause height measurements, Gage and Green (1982) suggested a technique from which stratospheric temperature gradients could be obtained directly from the power returns of a calibrated VHF radar. Such a technique could lead to a highly effective combination of active and passive sensors.

TABLE 7. System parameters for the VHF pulse-Doppler radar operated at Platteville, CO.*

Component	Parameter	Description
Antenna	type	Array of phased dipoles
	area	10^4 m^2
	beamwidth	2° (two way)
Transmitter	frequency	49.92 MHz
	peak power	15 kW
	pulse repetition frequency	625 Hz
	pulse width	16 μs
	range gate spacing	8 μs
Receiver	noise level	3 dB
	coherent integration	64 pulses

* Radar located 50 km north of Denver.

One of the advantages of radiometric Profilers is their ability to provide soundings at least every twenty minutes. However, data from United States polar orbiters include at most four soundings per day from the NOAA satellites and perhaps two soundings per day from the DMSP satellite. Thus, strictly speaking, only six combined soundings per day could be realized. However, retrieval strategies should be able to extend the time periods of useful soundings. One possibility is to use the combined sounding obtained at the time of satellite overflight as an initial guess for subsequent Profiler-only soundings. Another attractive possibility is to combine Profiler soundings with those obtained from the VAS sounders on geostationary satellites [Smith *et al.*, 1981]. This

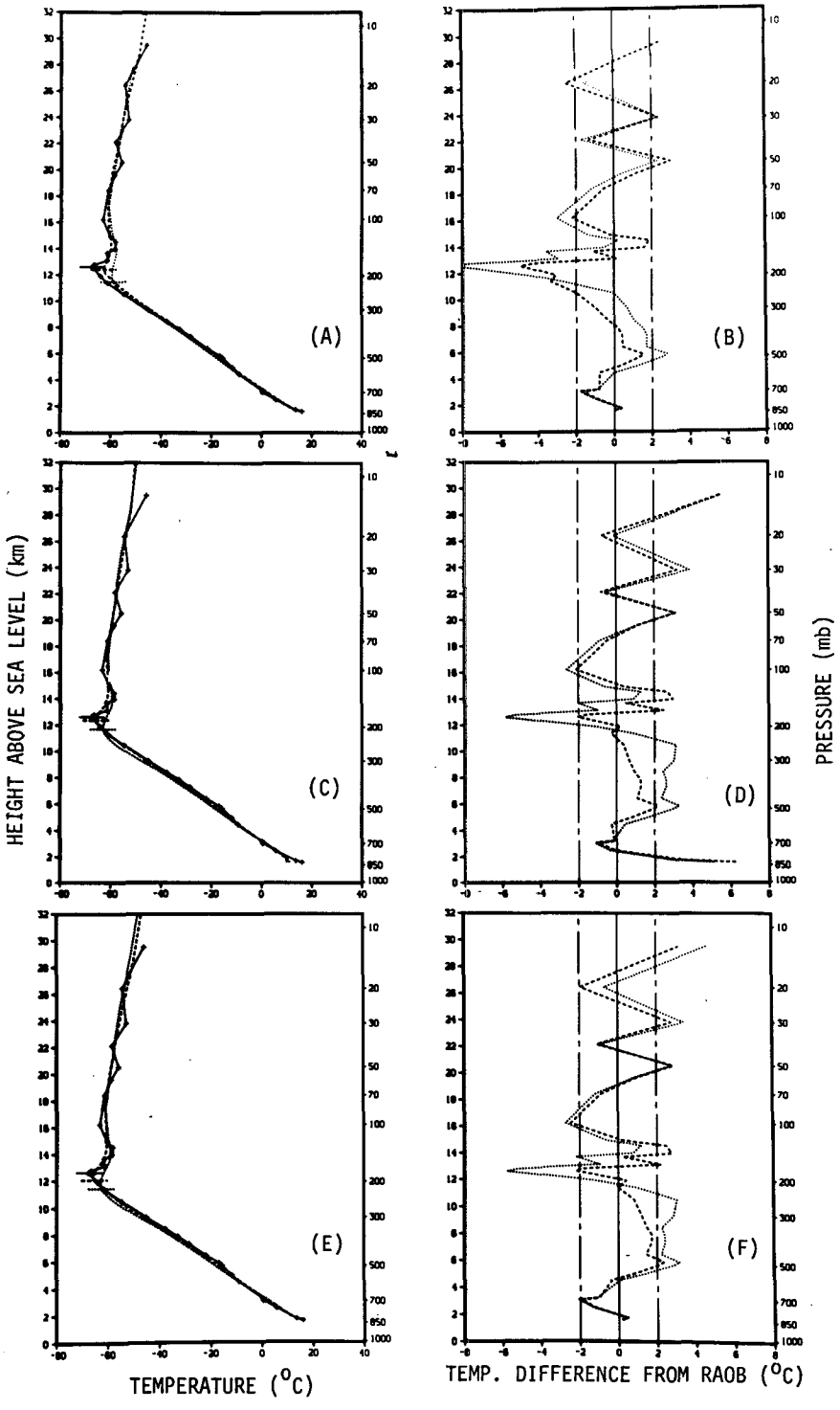

FIG. 7. Comparison of temperature profile from a RAOB and retrievals from VHF radar, Profiler and MSU data. (A, B) Profiler + VHF radar; (C, D) MSU + VHF radar; (E, F) Profiler + MSU + VHF radar. In the difference plots, the dotted curves refer to radiometric retrievals alone; the dashed curves refer to radiometric plus radar.

system has the potential of providing soundings every hour during clear conditions.

The results presented here are only a first step in determining the practical value of combining ground-based radiometric Profilers with satellite observations. Given that single-station accuracies are reliably deter-

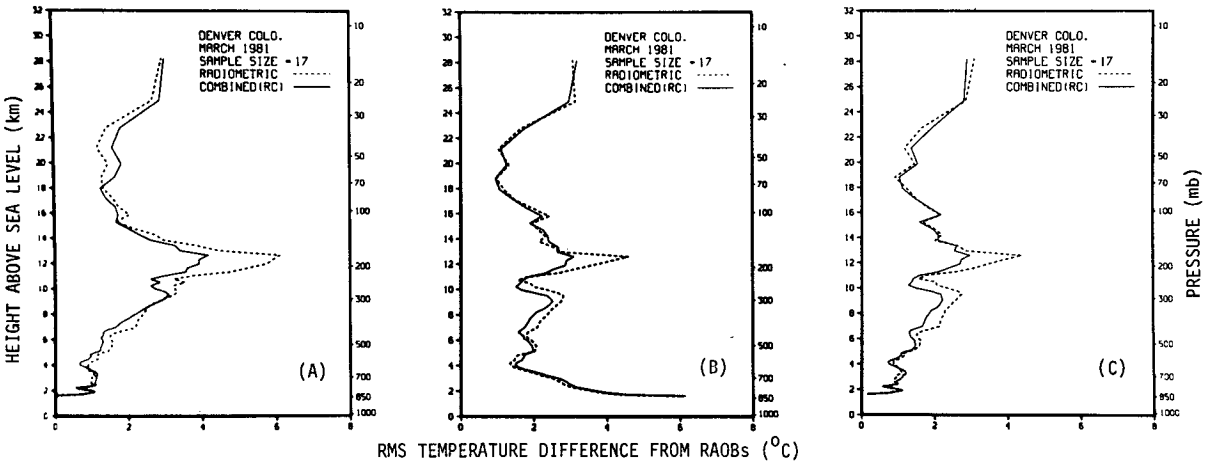

FIG. 8. The rms differences between temperature retrievals and NWS RAOBs. Curves labeled "combined" refer to radiometer + radar data. (A) Profiler + VHF radar; (B) MSU + VHF radar; (C) Profiler + MSU + VHF radar.

mined for various combinations of sensors, simulations can be performed to answer questions concerning the various tradeoffs involved in system design. Typical questions concern optimum placement of a limited number of Profilers, cost-benefit analyses, impact of Profiler temporal resolution on forecasting models, etc. Another area requiring extended investigation is the integration of the radar Profiler's winds with thermal soundings. As shown by Bleck *et al.* (1984), the vertical resolution of radiometrically retrieved profiles can be enhanced by using data obtained from a network of wind observations. Thus, the interplay of satellite and ground-based observations leads to a promising new variety of techniques to observe meteorological variables.

Acknowledgments. The authors thank Dr. Tom Schlatter for carefully reviewing the manuscript and Martin Decker for his assistance in obtaining Profiler data. The authors also express thanks to Dr. C. G. Little for his constant encouragement and interest during the performance of this work.

REFERENCES

Bleck, R., R. Brummer and M. Shapiro, 1984: Enhancement of remotely sensed temperature fields by wind observations from a VHF radar network. *Mon. Wea. Rev.*, **112**, 1795–1803.

Decker, M. T., E. R. Westwater and F. O. Guiraud, 1978: Experimental evaluation of ground-based microwave radiometric sensing of atmospheric temperature and water vapor profiles. *J. Appl. Meteor.*, **17**, 1788–1795.

Dongarra, J. J., J. R. Bunch, C. B. Moler and G. W. Steward, 1979: *LINPACK Users' Guide.* SIAM Publications, Philadelphia, PA, (see Introduction and Chapter 1).

Gage, K. S., and J. L. Green, 1979: Tropopause detection by partial specular reflection with very-high-frequency radar. *Science*, **203**, 1238–1239.

——, and ——, 1982: A technique for determining the temperature profile from VHF radar observations. *J. Appl. Meteor.*, **21**, 1146–1149.

Grody, N. C., 1983: Severe storm observation using the Microwave Sounding Unit. *J. Climate Appl. Meteor.*, **22**, 609–625.

Hoehne, W. E., 1980: Precision of National Weather Service upper air measurements. NOAA Tech. Memo. NWS T&ED-16. [NITS No. PB81-108136], 23 pp.

Hogg, D. C., M. T. Decker, F. O. Guiraud, K. B. Earnshaw, D. A. Merritt, K. P. Moran, W. B. Sweezy, R. G. Strauch, E. R. Westwater and C. G. Little, 1983a: An automatic profiler of the temperature, wind, and humidity in the troposphere. *J. Climate Appl. Meteor.*, **22**, 807–831.

——, F. O. Guiraud and E. R. Westwater, 1983b: Emission measurements at 31.6 GHz absorption by atmospheric water vapor. *Radio. Sci.*, **18**, 1295–1300.

Kendall, M. G., and A. Stuart, 1967: *The Advanced Theory of Statistics. Vol. 2*, Hafner, 690 pp. (see p. 386).

Little, C. G., 1982: Ground-based remote sensing for meteorological nowcasting. *Nowcasting*, K. A. Browning, Ed., Academic Press, 65–85.

Phillips, N. A., L. M. McMillin, D. Q. Wark and A. Gruber, 1979: An evaluation of early operational temperature soundings from TIROS-N. *Bull. Amer. Meteor. Soc.*, **60**, 1188–1197.

Rosenkranz, P. M., 1975: Shape of the 5 mm oxygen band in the atmosphere. *IEEE Trans. Antennas Propag.*, **23**, 498–506.

Smith, W. L., M. Woolf, C. M. Hayden, D. Q. Wark and L. M. McMillin, 1979: The TIROS-N operational vertical sounder. *Bull. Amer. Meteor. Soc.*, **60**, 1177–1187.

——, V. E. Suomi, W. P. Menzel, H. M. Woolf, L. A. Sromovsky, H. E. Revercomb, C. M. Hayden, D. N. Erickson and F. R. Mosher, 1981: First sounding results from VAS-D. *Bull. Amer. Meteor. Soc.* **62**, 232–236.

Strand, O. N., and E. R. Westwater, 1968: Minimum rms estimation of the numerical solution of a Fredholm integral equation of the first kind. *SIAM J. Numer. Anal.*, **5**, 287–295.

Westwater, E. R., and N. C. Grody, 1980: Combined surface- and satellite-based microwave temperature profile retrieval. *J. Appl. Meteor.*, **19**, 1438–1444.

——, M. T. Decker, A. Zachs and K. S. Gage, 1983: Ground-based remote sensing of temperature profiles by a combination of microwave radiometry and radar. *J. Climate Appl. Meteor.*, **22**, 126–133.

——, W. B. Sweezy, L. M. McMillin and C. Dean, 1984: Determination of atmospheric temperature profiles from a statistical combination of ground-based Profiler and operational NOAA 6/7 satellite retrievals. *J. Climate Appl. Meteor.*, **23**, 689–703.